Topola Poplar SINCE 1957

OPEN ACCESS

DOI: 10.5937/topola2617005V
UDC: 630*57(497.113)

Original scientific paper

A Sentinel-based remote sensing framework for integrating ICP Forests Level II observations in forest health assessment in Serbia

Vladimir Višacki[1]*, Milan Drekić[1], Lazar Jeftić[1], Bratislav Matović[1], Lazar Kesić[1], Lazar Pavlović[2], Saša Orlović[1]

[1] University of Novi Sad, Institute of Lowland Forestry and Environment, Novi Sad, Serbia
[2] University of Novi Sad, Faculty of Agriculture, Novi Sad, Serbia

* Corresponding author: Vladimir Višacki; E-mail: vladimir.visacki@uns.ac.rs

Received: 17 April 2026; **Revised:** 3 June 2026; **Accepted:** 15 June 2026

Abstract: Forest condition assessment based only on field observations can be limited when crown deterioration is not clearly linked to recorded damage. This study integrates ICP Forests Level II terrestrial observations with multi-sensor Earth Observation (EO) data to assess forest condition at two Serbian monitoring plots, Odžaci and Fruška Gora, during the 2025 growing season. Field data included crown defoliation, defoliation classes and tree damage records, while EO indicators included Sentinel-2 vegetation, moisture and disturbance indices, Sentinel-1 radar backscatter and MODIS daytime land surface temperature.

ICP observations showed poorer crown condition at Odžaci, with higher mean and median defoliation than Fruška Gora (35.5% and 30.0% vs. 24.1% and 15.0%), fewer trees in the low-defoliation class, and more frequent recorded damage.

EO indicators showed statistically supported consistency with this terrestrial pattern. Mean Sentinel-2 greenness indices were similar between plots, including NDVI (0.858 ± 0.042 at Odžaci vs. 0.859 ± 0.036 at Fruška Gora) and NDMI (0.329 ± 0.044 vs. 0.329 ± 0.037), but seasonal trajectories were more informative. NDMI declined more strongly at Odžaci (−0.0289 vs. −0.0217 month^{-1}; $p = 0.046$), while MSI (+0.0332 vs. +0.0245 month^{-1}; $p = 0.033$) and BSI (+0.0297 vs. +0.0208 month^{-1}; $p = 0.020$) increased more strongly. MODIS daytime LST was also significantly higher at Odžaci (28.49 ± 4.94°C) than at Fruška Gora (23.64 ± 4.69°C; $p < 0.001$), and Sentinel-1 VH and VV backscatter were significantly lower at Odžaci.

The results show that satellite-derived indicators, particularly NDMI, MSI, BSI, MODIS LST and Sentinel-1 backscatter, were statistically consistent with field-assessed crown condition at Odžaci. EO data therefore complemented ICP Forests observations by identifying moisture, thermal and structural signals associated with field-observed crown deterioration. The results should be interpreted as a pilot-scale ICP–EO consistency assessment rather than a regional validation or direct causal attribution of drought.

Keywords: ICP Forests Level II, Sentinel-2, Sentinel-1, MODIS LST, canopy defoliation, moisture stress, forest health, Serbia.

Copyright © 2026 Institute of Lowland Forestry and Environment.
This is an Open Access paper distributed under the terms of the Creative Commons Attribution 4.0 International (CC-BY 4.0) License.

1. Introduction

Forests provide essential ecosystem services, including carbon sequestration, climate regulation through biophysical feedbacks (e.g. albedo and evapotranspiration), biodiversity conservation, and protection against natural hazards. However, forest ecosystems are increasingly exposed to interacting pressures from climate change and air pollution, resulting in chronic stress, disturbance amplification, and more frequent episodes of decline and mortality (Stojanovic et al. 2021). In Europe, rising temperatures, altered precipitation regimes, and increasing frequency of drought and heat extremes are widely recognized as major drivers of reduced vitality and forest dieback, often interacting with additional stressors such as nitrogen deposition, tropospheric ozone, pests, pathogens, and legacy effects of past management (de la Cruz et al. 2014; Galic et al. 2018; Gessler et al. 2022). These stressor interactions are complex and frequently non-linear, making it challenging to distinguish gradual decline from abrupt disturbance impacts and to attribute observed changes to specific drivers (Pavlovic et al. 2017).

Long-term, standardized ground-based monitoring is therefore essential for detecting trends, diagnosing causes, and supporting adaptive forest management and policy decisions. In Europe, the International Co-operative Programme on Assessment and Monitoring of Air Pollution Effects on Forests (ICP Forests) represents one of the most comprehensive transnational forest monitoring networks worldwide (Eichhorn et al. 2020). It provides harmonized information on crown condition, growth, deposition, soil and foliage chemistry, and multiple indicators of forest functioning (Bussotti et al. 2024; Galic et al. 2025; Gessler et al. 2022). ICP Forests operates at two complementary levels. Level I consists of a large-scale systematic grid of plots primarily focused on crown condition assessment and damage symptoms, allowing representative evaluation of spatial and temporal variability in forest condition. Level II comprises intensive monitoring plots designed to investigate cause–effect relationships between forest condition and environmental stressors through detailed measurements of tree growth, foliar chemistry, soil properties, atmospheric deposition, and ecosystem processes (Gessler et al. 2022; Vasic et al. 2020). Since defoliation is not a cause-specific indicator of tree vitality, its interpretation benefits from additional physiological, environmental, and remotely sensed indicators that help distinguish between biotic damage, drought stress, and broader site-related effects (Bussotti et al. 2024). Annual technical assessments provide a consistent overview of forest condition across Europe and repeatedly identify drought and biotic disturbances among the dominant drivers of damage (Michel et al. 2022).

Despite their scientific robustness, ground-based monitoring networks face practical limitations. Field surveys are labor-intensive, costly, and spatially sparse relative to the landscape scale at which disturbances unfold. Many crown condition indicators rely partly on expert assessment and are difficult to upscale to regional or national levels. Furthermore, annual or multi-year observation cycles may not capture within-season stress dynamics or rapidly developing disturbance events. For these reasons, there is growing consensus that ground-based monitoring should be complemented by Earth Observation (EO) systems capable of providing spatially continuous and temporally frequent information (Ferretti et al. 2024; Guerrieri et al. 2025).

Remote sensing (RS) has become a central tool in forest health assessment because it enables repetitive, synoptic, and objective observation of canopy condition. The contribution of RS to drought impact assessment has been recognized for decades, particularly for mapping spatial patterns of stress and quantifying recovery trajectories (Deshayes et al. 2006). Modern multispectral, radar, and LiDAR sensors capture stress-related changes through variations in canopy reflectance, structure, and moisture status. The conceptual framework of "spectral traits" and "spectral trait variations" emphasizes that environmental stress modifies canopy biochemical and structural properties, which can be detected as changes in spectral signals across space and time (Lausch et al. 2016, 2017). However, similar spectral responses may arise from different stressors, limiting causal interpretation when RS is used in isolation. Consequently, multiple reviews underline the necessity of integrating RS with

standardized in situ measurements to ensure ecological validity and operational applicability (Drechsel and Forkel, 2025; Pause et al. 2016).

Empirical studies increasingly demonstrate the value of combined ground and RS approaches. For example, Moreno-Fernández et al. (2022) integrated dendrochronological tree-ring data with satellite-derived greenness and wetness indices to analyze drought-induced dieback in Mediterranean pine forests. Their results showed that tree growth and spectral trajectories provide complementary information, with drought impacts often more pronounced in radial growth than in canopy spectral indices. Such multiscale analyses highlight the importance of integrating tree-level and stand-level indicators to disentangle mechanisms driving forest decline. This approach is particularly relevant within the ICP Forests framework, where plot-based assessments of defoliation and damage can be contextualized using spatially continuous RS indicators.

The Copernicus Sentinel missions provide an especially strong foundation for operational integration with ICP Forests data. Sentinel-2 MSI provides 13 spectral bands, including 10 m visible and near-infrared bands and 20 m red-edge and short-wave infrared bands, which are widely used for vegetation and forest-cover change assessment (Drusch et al 2012; Pelc-Mieczkowska et al. 2021). Sentinel-1 radar imagery adds structural and moisture-related information independent of cloud conditions (Hellwig et al. 2026; Paluba et al. 2025), while Sentinel-3 (ESA 2024) and Sentinel-5P provide complementary data on land surface temperature (Ghent et al. 2024) and atmospheric pollutants, respectively (Hoek van Dijke et al. 2023). Together, these missions support multi-sensor analyses linking canopy condition, climatic stress, and pollution exposure (Le et al. 2024).

Recent studies explicitly connecting Sentinel data with ICP Forests plots demonstrate the feasibility of such integration. Molnár et al. (2025) combined Sentinel-2 imagery, Google Earth Engine cloud processing, and ICP Forests Level I and Level II observations in Hungary to produce standardized NDVI anomaly maps and classify forest health severity. Their results showed agreement between satellite-derived anomaly classes and field-based defoliation assessments, confirming the usefulness of Sentinel-2 time series for complementing ICP Forests monitoring. Similarly, Alekseev and Chernikhovskii (2022) demonstrated that statistical processing of Sentinel-2 data together with ICP-style plot information enables scaling of forest condition assessment from plot samples to regional mapping using machine learning approaches (Estrada et al. 2023). Beyond crown condition, ICP Forests data have also been used to calibrate RS-derived ecological traits. Loozen et al. (2020) successfully mapped canopy nitrogen across European forests using remotely sensed predictors combined with environmental variables and ICP calibration data, illustrating how plot networks can anchor continent-scale modelling efforts. Sentinel-2 time-series and change-detection approaches have been successfully applied for detecting both gradual drought-related forest decline and sudden disturbance events, particularly when supported by higher-resolution validation data (Ács et al. 2026; Vulova et al. 2025).

Level II measurements such as leaf area index (LAI) further support integration workflows. Operational LAI determination at ICP Level II plots following standardized protocols provides reliable ground reference data that can be compared with satellite-derived biophysical products (Mitrović et al. 2021). Moreover, studies analyzing spectral index sensitivity to defoliation (Marx and Kleinschmit, 2017) demonstrate that combining vegetation indices (NDVI and red-edge-based metrics) can improve discrimination across stress severity gradients. Because individual vegetation indices may be primarily sensitive to specific canopy properties, such as greenness or water content, multi-index approaches are often preferred for vegetation health assessment under combined stress conditions (Kumar et al. 2025). Long-term structural mapping using multi-sensor synergies, including multispectral and LiDAR data, also shows that satellite time series can capture trends in biomass, canopy cover, and height (Matovic et al. 2024; Tanase et al. 2024), reinforcing the potential of RS for monitoring structural forest attributes.

Despite rapid technological advances, systematic implementation of RS-based forest health assessment aligned with ICP standards remains limited (Drechsel and Forkel, 2025). The literature consistently emphasizes that future forest monitoring systems must integrate long-term ground observations with EO products to achieve scalable, comparable, and policy-relevant assessments (Ferretti et al. 2024; Guerrieri et al. 2025). The central methodological challenge is to harmonize field-

measured parameters and satellite-derived proxies, ensuring conceptual alignment, reproducibility, and uncertainty awareness.

Although the individual EO indicators used in this study are well established, their structured application to Serbian ICP Forests Level II plots provides a pilot case for operationally linking national ground-based forest monitoring with spatially continuous Sentinel-derived indicators. Against this background, the present study aims to apply and evaluate a plot-scale ICP–EO integration workflow at two Serbian ICP Forests Level II plots for the 2025 growing season. Specifically, the study seeks to (i) establish a conceptual linkage between field-measured ICP variables and satellite-derived proxies, (ii) evaluate the consistency between ground-based observations and EO indicators, and (iii) explore the most likely stress signatures associated with canopy condition at the two study sites, based on the combined interpretation of field observations and EO-derived indicators. Therefore, the novelty of this study lies not in the development of a new spectral index or sensor-specific algorithm, but in the plot-scale implementation and evaluation of an ICP–EO integration workflow under Serbian monitoring conditions.

A key component of this study is the explicit linkage between ICP variables and EO proxies, which enables consistent interpretation across observation scales and forms the conceptual basis of the integration framework. By systematically comparing EO-derived indicators with field observations, the study contributes to bridging the gap between standardized ground monitoring and spatially continuous remote sensing-based assessment. Rather than replacing ICP monitoring, satellite data are treated as a complementary layer that enhances spatial representativeness, temporal resolution, and the detection of environmental stress signals, while field observations provide ecological interpretation and validation (Gessler et al. 2022; Molnár et al. 2025; Pause et al. 2016).

2. Material and methods

2.1. Study plots, ICP Forests data and EO datasets

This study was conducted at two ICP Forests Level II monitoring plots in Serbia: Fruška Gora (FG; 45.1569087° N, 19.8113405° E, Figure 1) and Odžaci (ODZ; 45.4553233° N, 19.1737379° E, Figure 2). The analysis integrates terrestrial ICP Forests observations with multi-sensor Earth Observation (EO) data for the 2025 growing season.

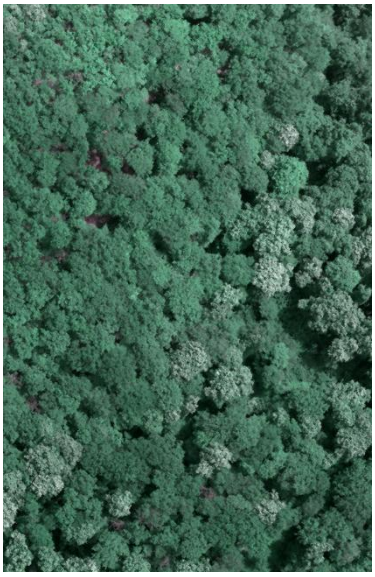

Figure 1. RGB drone overview of the Fruška Gora ICP Forests Level II monitoring plot.

Figure 2. RGB drone overview of the Odžaci ICP Forests Level II monitoring plot.

ICP Forests data included tree-level crown condition and damage observations. Crown condition was represented by defoliation values and defoliation classes, while damage information included tree damage records and damage intensity. Tree-level crown-condition and damage records were linked using unique tree identifiers, and only trees with matched records were included in the direct field-data comparison. For EO integration, tree-level ICP observations were aggregated to the plot level and used as terrestrial reference information for interpreting satellite-derived indicators.

EO datasets were selected according to their sensitivity to canopy condition, availability during the 2025 growing season, and suitability for plot-scale extraction. Sentinel-2 multispectral imagery was used as the main optical dataset. Reflectance bands in the visible, red-edge, near-infrared and short-wave infrared domains were used to derive vegetation, pigment, moisture and disturbance-related indices. Sentinel-1 C-band SAR data were used to complement optical observations with radar-based information on canopy structure and moisture-related scattering properties. VV and VH backscatter coefficients were derived from Ground Range Detected products and expressed in decibels. MODIS daytime land surface temperature was used as the thermal indicator because of its high temporal frequency and suitability for seasonal thermal characterization.

EO indicators were extracted at the plot level using buffer-based sampling around the ICP plot coordinates. Sentinel-2 and Sentinel-1 variables were extracted using a 50 m plot buffer, while MODIS LST was extracted using a 1000 m buffer to account for the coarser spatial resolution of the thermal product. Sentinel-2 observations were cloud-masked before index calculation, and only valid observations from May to September 2025 were retained for the seasonal EO analysis. For each valid observation date and plot, EO values were summarized using mean values, while standard deviation was used where applicable to describe variability.

To document the EO data basis used for statistical analysis, the number of valid observations retained for each sensor and plot is summarized in Table 1. The analysis was restricted to the May–September 2025 growing season in order to capture peak canopy activity and late-season stress development. For each valid date, satellite values were extracted within the plot buffer and summarized to a plot-level value. These plot-level time series were then used to calculate seasonal means, standard deviations and monthly trends.

2.2. EO-derived indicators and ICP–EO conceptual linkage

EO-derived indicators were selected to represent canopy greenness, photosynthetic activity, pigment and chlorophyll status, canopy moisture, moisture stress, surface/canopy opening, productivity-related canopy function, thermal environment, and radar-based structural or moisture-related properties. Sentinel-2 multispectral bands in the visible, red-edge, near-infrared (NIR), and short-wave infrared (SWIR) domains were used to calculate vegetation, moisture, pigment, and disturbance-related indices. Sentinel-1 VV and VH backscatter were used as radar indicators of canopy structure and moisture-related scattering, while MODIS daytime land surface temperature (LST Day) was used as a contextual thermal indicator.

The following Sentinel-2 indices and proxies were calculated:

NDVI – Normalized Difference Vegetation Index

$$NDVI = (NIR - Red) / (NIR + Red)$$

NDVI was used as an indicator of canopy greenness and photosynthetic activity. It is widely applied in vegetation and forest monitoring, although its sensitivity may decrease in dense forest canopies because of saturation effects (Huang et al. 2021; Huete, 2012; Yan et al. 2025).

EVI – Enhanced Vegetation Index

$$EVI = 2.5 \times (NIR - Red) / (NIR + 6 \times Red - 7.5 \times Blue + 1)$$

EVI was used as an additional greenness and canopy-activity indicator because it reduces atmospheric and soil-background effects and improves sensitivity in high-biomass vegetation compared with NDVI (Huete, 2012; Yan et al. 2025).

Table 1. Earth Observation datasets used for plot-level extraction during the 2025 growing season.

EO dataset	Period used	Temporal basis	Valid observations used in analysis	Spatial resolution/ extraction buffer	Variables derived	Aggregation used
Sentinel-2 MSI	May–September 2025	Cloud-masked valid observations during growing season	FG: 50; ODZ: 29	10–20 m bands; 50 m plot buffer	NDVI, EVI, NDRE, CIred-edge, MTCI, NDMI, MSI, BSI, FAPAR proxy, productivity proxy	Mean value per valid date and plot; seasonal mean ± SD; linear monthly trend
Sentinel-1 SAR	May–September 2025	Available VV/VH GRD acquisitions	FG: 76; ODZ: 76	~10 m; 50 m plot buffer	VH and VV backscatter	Mean value per valid date and plot; seasonal mean ± SD; Mann–Whitney U comparison
MODIS LST Day	May–September 2025	Valid daytime LST observations	FG: 101; ODZ: 105	~1 km; 1000 m plot buffer	Daytime land surface temperature	Mean value per valid date and plot; seasonal mean ± SD; Mann–Whitney U comparison
MODIS vegetation/biophysical products	May–September 2025	Available valid product observations	NDVI/EVI: FG: 10, ODZ: 10; LAI/FPAR: FG: 39, ODZ: 39	Product-dependent; plot-level extraction	LAI proxy, FAPAR proxy and productivity-related proxy	Seasonal mean ± SD and exploratory trend comparison

Note: Valid observations refer to observations retained after sensor-specific preprocessing, cloud masking or quality filtering. For each valid observation date, EO values were extracted within the corresponding plot buffer and summarized at plot level. The reported mean ± SD values in the Results represent temporal variability among valid observations during May–September 2025, after plot-level extraction, rather than raw pixel-level spatial variability.

NDRE – Normalized Difference Red Edge Index

NDRE = (NIR − Red-edge) / (NIR + Red-edge)

NDRE was used as a red-edge indicator sensitive to chlorophyll content and subtle physiological changes in vegetation. Red-edge indices are particularly useful for detecting canopy stress before strong changes are visible in broad greenness indices (Kumar et al. 2025; Yan et al. 2025).

CIred-edge – Chlorophyll Index Red Edge

CIred-edge = (NIR / Red-edge) − 1

CIred-edge was used as an additional chlorophyll-sensitive index, providing information on pigment-related canopy condition and potential physiological stress (Kumar et al. 2025; Yan et al. 2025).

MTCI – MERIS Terrestrial Chlorophyll Index

MTCI = (NIR − Red-edge2) / (Red-edge2 − Red-edge1)

MTCI was used as a chlorophyll-related index based on the red-edge spectral region. In this study, it was interpreted as an additional pigment-sensitive indicator of canopy physiological condition, complementary to NDRE and CIred-edge (Yan et al. 2025; Kulesza et al. 2025).

NDMI – Normalized Difference Moisture Index

NDMI = (NIR − SWIR1) / (NIR + SWIR1)

NDMI was used as an indicator of canopy water content and moisture-related stress. Because SWIR reflectance is sensitive to vegetation water content, NDMI is suitable for detecting changes in canopy moisture status (Deshayes et al. 2006; Gao, 1996; Le et al. 2024).

MSI – Moisture Stress Index

MSI = SWIR1 / NIR

MSI was used as a moisture-stress indicator. Higher MSI values indicate lower canopy water content and stronger moisture stress. It was interpreted together with NDMI to evaluate seasonal moisture limitation at the plot scale (Kumar et al. 2025; Le et al. 2024; Yan et al. 2025).

BSI – Bare Soil Index

BSI = (SWIR1 + Red − NIR − Blue) / (SWIR1 + Red + NIR + Blue)

BSI was used as an exploratory indicator of bare soil exposure, canopy opening, or mixed soil–vegetation signal. Higher BSI values were interpreted as stronger surface exposure or canopy-opening signal, particularly when considered together with defoliation and moisture indicators (Le et al. 2024; Yan et al. 2025).

FAPAR proxy – Fraction of Absorbed Photosynthetically Active Radiation proxy

FAPAR proxy = EO-derived canopy absorption proxy based on Sentinel-2 vegetation-index response

The FAPAR proxy was used as an exploratory indicator of canopy functional activity and absorbed photosynthetically active radiation. It was interpreted only in relative terms between plots and through seasonal dynamics, not as a direct biophysical FAPAR validation product. FAPAR and related canopy-function indicators are commonly used to describe vegetation productivity and photosynthetic functioning in remote-sensing-based forest assessment (Huete, 2012; Tigabu and Gessesse, 2025; Yan et al. 2025).

Productivity proxy

Productivity proxy = NDVI × NDMI

The productivity proxy was used as an exploratory indicator combining canopy greenness and canopy moisture status. Lower values or stronger seasonal decline were interpreted as reduced canopy functional condition. This proxy was not treated as a direct estimate of carbon productivity, but as a relative plot-scale indicator of vegetation condition combining greenness and water-status information (Gao, 1996; Huete, 2012; Yan et al. 2025).

MODIS LST Day – daytime land surface temperature

MODIS daytime land surface temperature was used as a contextual thermal indicator. LST values were converted to degrees Celsius and interpreted as indicators of the daytime surface thermal environment. Higher LST may indicate reduced canopy cooling, lower evapotranspiration, increased surface exposure, or a combination of these processes. Therefore, LST was used to support the interpretation of thermal and moisture-related stress, but not as direct proof of drought causality (Deshayes et al. 2006; Ghent et al. 2024; Hoek van Dijke et al. 2023).

Sentinel-1 VH and VV backscatter

Sentinel-1 VH and VV backscatter coefficients were used as radar-based indicators of canopy structure and moisture-related scattering properties. Backscatter values were expressed in decibels (dB). These variables were interpreted cautiously because radar response depends on canopy architecture, biomass distribution, surface moisture, acquisition geometry, and phenological conditions. Nevertheless, optical–radar integration is useful for forest structure, moisture, and condition assessment (Paluba et al. 2025; Tanase et al. 2024; Vafaei et al. 2021).

To ensure conceptual consistency between terrestrial ICP Forests observations and satellite-derived indicators, a systematic linkage between ICP variables and EO proxies was established (Table 2). The table presents a broader integration framework showing how different ICP Level II observations may be linked with spectral, radar, thermal, atmospheric and productivity-related EO indicators. In the present study, the statistical analysis was focused on crown condition, defoliation classes and damage records, while EO indicators were used to characterize canopy greenness, pigment status, moisture condition, surface exposure, thermal environment and radar-based structural or moisture-related properties. Other variables listed in Table 2, such as atmospheric exposure, foliar chemistry, biomass and growth-related indicators, are included as potential extensions of the ICP–EO framework, but were not used for statistical inference in this pilot analysis.

Table 2. Conceptual framework for linking ICP Forests Level II variables with EO-derived proxies (Le et al. 2024).

A) Foliage chemistry and canopy condition					
ICP Level II variable	**Unit**	**What it represents**	**EO proxy**	**Satellite**	**Meaning / interpretation**
Foliar nitrogen (N)	%	Nutrient status linked to photosynthetic capacity	NDRE; red-edge metrics	Sentinel-2	Red-edge indices often co-vary with pigment/nutrient-related signals
Leaf chlorophyll	mg/cm²	Pigment pool and photo-synthetic apparatus status	CI(RE), NDRE	Sentinel-2	Chlorophyll-sensitive red-edge indices
Pigment stress	relative	Chlorophyll degradation/ physiological stress	NDRE/CI(RE) decline (optional anomalies)	Sentinel-2	Reduced pigment signal under stress
Leaf/canopy water status	%	Water content/ drought impact	NDMI, MSI	Sentinel-2	Moisture/water stress sensitivity
LAI (if measured)	m²/m²	Canopy leaf area and structure	Sentinel-2 LAI product	Sentinel-2	Biophysical canopy density product
B) Soil / surface condition (context + site-level stress)					
ICP Level II variable	**Unit**	**What it represents**	**EO proxy**	**Satellite**	**Meaning / interpretation**
Soil moisture (surface/near-surface)	m³/m³	Water availability/ wetness	VV/VH backscatter (optional)	Sentinel-1	Radar sensitivity to moisture + structure (context-dependent)
Surface disturbance / bare soil exposure	index	Open soil patches, disturbance mixtures	BSI	Sentinel-2	Higher BSI = more bare soil exposure
Thermal stress context	°C	Heating/ dryness context	LST product	Sentinel-3 / Landsat	Higher LST can reflect hotter/drier conditions

Table 2. Continue.

C) Atmospheric pollution exposure (drivers)					
Exposure proxy	**Unit**	**What it represents**	**Product**	**Satellite**	**Interpretation**
NO_2 column	mol/m² (typical)	Spatial gradient of NOx-related pollution	Tropospheric NO_2 column	Sentinel-5P	Used as a driver/exposure proxy
SO_2 column	mol/m² (typical)	SOx exposure gradient	SO_2 column	Sentinel-5P	Driver/exposure proxy
O_3-related product	DU	Broad ozone-related proxy	O_3 product	Sentinel-5P	Exposure proxy with known limitations
Aerosols	AOD	Aerosol loading context	AOD	Sentinel-3	Contextual atmospheric driver
D) Climate stress context					
Variable	**Unit**	**EO proxy**	**Satellite**	**Interpretation**	
Temperature context	°C	LST	MODIS / Sentinel-3 / Landsat	Proxy for thermal environment	
Drought intensity context	index	NDMI seasonal dynamics; MSI	Sentinel-2	Moisture limitation proxy	
E) Growth, biomass, productivity (optional layers depending on available plot data)					
Variable	**Unit**	**EO proxy**	**Satellite**	**Interpretation**	
Aboveground biomass	t/ha	SAR + optical combined proxy (optional)	Sentinel-1 + Sentinel-2	Requires model-based estimation	
Productivity	gC/m²/yr	FAPAR-based proxy (optional)	Sentinel-2	Model-driven productivity proxy	
DBH increment	mm/yr	NDVI seasonal metrics (optional)	Sentinel-2	Proxy only; indirect	

List of Abbreviations: EO: Earth Observation; RS: Remote sensing; MSI: MultiSpectral Instrument (Sentinel-2); SAR: Synthetic Aperture Radar (Sentinel-1); NIR: Near-infrared; SWIR: Short-wave infrared; NDVI, EVI, NDMI, NDRE, MSI, CI(RE), NBR, BSI: vegetation indices (defined above); LAI: Leaf Area Index; FAPAR: Fraction of Absorbed Photosynthetically Active Radiation; LST: Land Surface Temperature. The relationships defined in Table 2 were used to guide the selection and interpretation of EO-derived indicators. The quantitative ICP–EO comparison was restricted to variables available for both plots during the 2025 growing season.

Note: The table shows the broader potential for ICP–EO integration. The quantitative analysis in this study used ICP crown condition and damage records, Sentinel-2 indices, Sentinel-1 VH/VV backscatter and MODIS daytime LST. Atmospheric exposure variables, foliar chemistry, biomass and growth-related indicators were included as conceptual extensions but were not analyzed statistically.

2.3 Statistical analysis

Descriptive statistics were calculated for ICP and EO-derived variables. For ICP field observations, tree-level data were summarized at the plot level using mean and median defoliation, defoliation classes, and the proportion of trees with non-zero damage records. Differences between plots in categorical ICP variables were evaluated using Fisher's exact test because of the small sample size and categorical structure of the data. In the statistical tables, mean ± SD values represent temporal

variability among valid observation dates during May–September 2025, after plot-level extraction for each date. Therefore, these values should be interpreted as seasonal temporal variability rather than within-plot spatial variability, unless explicitly stated otherwise.

EO-derived indicators were analyzed for the May–September 2025 growing-season period. For each plot and indicator, valid observations were summarized using mean and standard deviation. Between-plot differences in EO indicator distributions were evaluated using the Mann–Whitney U test. Seasonal EO trends were calculated using linear regression slopes for each indicator and plot, expressed as index units per month. For MODIS daytime LST, slopes were expressed as °C per month. Differences in seasonal trends between Odžaci and Fruška Gora were evaluated using a site × time interaction term. EO preprocessing and extraction were performed in Google Earth Engine, while statistical analyses and tabular summaries were performed in Python. Statistical tests included Fisher's exact test, Mann–Whitney U tests and linear regression models with site × time interaction.

Because only two ICP Forests Level II plots were included, formal correlation analysis between plot-level ICP variables and EO indicators was not used for statistical inference. Instead, the relationship between terrestrial and satellite observations was evaluated using an exploratory ICP–EO consistency assessment. Odžaci was treated as the plot with poorer field-assessed crown condition based on higher defoliation and more frequent recorded damage. EO indicators were then evaluated according to whether they showed the expected response at Odžaci relative to Fruška Gora. For greenness, pigment, moisture and productivity-related indicators, the expected response was lower values or stronger seasonal decline. For moisture-stress, disturbance, thermal and radar indicators, the expected response was stronger seasonal increase, higher LST, or altered/lower radar backscatter. Statistical significance was evaluated at $p<0.05$, and all results were interpreted as exploratory plot-scale evidence rather than regional validation or causal attribution.

3. Results

3.1. Integrated field and remote sensing assessment of canopy condition

The integrated analysis of field observations and satellite-derived indicators revealed a clear difference in crown condition between the two study plots, while also showing that field-recorded damage alone did not fully explain the observed defoliation pattern. The combined dataset indicated an EO pattern consistent with moisture limitation and thermal stress, especially at the Odžaci site. Crown condition (TRC/TRE) refers to defoliation-based assessments, while TRD/TRF variables describe damage symptoms and identified causal agents.

Field observations indicated poorer crown condition at Odžaci compared with Fruška Gora. Odžaci had higher mean and median defoliation, a lower proportion of trees in the low-defoliation class (<25%), and a higher proportion of trees in the moderate defoliation class (25–59%). Fisher exact tests confirmed a significant difference in the proportion of trees with low defoliation (<25%; $p = 0.040$) and in the proportion of trees with non-zero TRD records ($p < 0.001$). The difference in the proportion of trees with moderate defoliation was marginal ($p = 0.054$), while differences in severely defoliated trees (≥60%) and completely defoliated trees were not statistically significant. Nevertheless, both severe and complete defoliation were numerically more frequent at Odžaci, suggesting a less favorable crown condition at this plot (Table 3).

Although damage records were more frequent at Odžaci, the dominant damage intensity remained low to moderate. This indicates that higher defoliation was not fully proportional to recorded damage intensity, supporting the need to interpret ICP crown condition together with EO-derived indicators of canopy moisture, thermal conditions, and structural change.

Sentinel-2 optical indicators showed generally similar mean values between the two plots during the May–September 2025 growing season (Table 4). Mean NDVI was almost identical at Fruška Gora and Odžaci (0.859 ± 0.036 vs. 0.858 ± 0.042; $p = 0.883$), indicating that average canopy greenness did not clearly separate the two plots. However, the seasonal NDVI trend was more negative at Odžaci than at

Fruška Gora (−0.0142 vs. −0.0053 month^{-1}), suggesting a stronger seasonal decline in greenness at the plot with poorer ICP crown condition, although the difference in slope was not statistically significant (interaction p = 0.157).

Table 3. TRC–TRD summary and exploratory statistical comparison between plots.

Indicator	Fruška Gora	Odžaci	Difference	Statistical test	p-value	Interpretation
Number of trees	40	38	-	-	-	-
Mean defoliation (%)	24.1	35.5	+11.4	Descriptive	-	Higher mean defoliation at Odžaci
Median defoliation (%)	15.0	30.0	+15.0	Descriptive	-	Higher median defoliation at Odžaci
Trees with defoliation <25%	27 (67.5%)	16 (42.1%)	−25.4 pp	Fisher exact test	0.040	Significantly fewer low-defoliation trees at Odžaci
Trees with defoliation 25–59%	9 (22.5%)	17 (44.7%)	+22.2 pp	Fisher exact test	0.054	Marginally higher moderate defoliation at Odžaci
Trees with defoliation ≥60%	4 (10.0%)	5 (13.2%)	+3.2 pp	Fisher exact test	0.734	Not significant
Trees with 100% defoliation	1 (2.5%)	4 (10.5%)	+8.0 pp	Fisher exact test	0.195	Not significant
Trees with non-zero TRD record	27 (67.5%)	38 (100.0%)	+32.5 pp	Fisher exact test	<0.001	Significantly more trees with recorded damage at Odžaci
Dominant intensity	Mostly 1	Mostly 1-2	-	Descriptive	-	Low-intensity damage dominates at both plots
Extreme intensity	3 trees class 6; 1 tree class 7	4 trees class 7	-	Descriptive	-	Mortality more frequent at Odžaci

Note: Fisher exact tests were applied to categorical tree-count data because of small group sizes. Mean and median defoliation values are presented descriptively in this table; categorical defoliation classes were used for statistical comparison because they directly correspond to the ICP crown-condition classification used in the plot-level assessment.

A similar pattern was observed for EVI and red-edge indicators. Mean EVI was slightly higher at Odžaci than at Fruška Gora (0.645 ± 0.070 vs. 0.635 ± 0.083; p = 0.467), while both plots showed a declining seasonal trend, with a somewhat stronger decrease at Odžaci (−0.0462 vs. −0.0398 month^{-1}; interaction p = 0.483). Mean NDRE values were also very similar between Odžaci and Fruška Gora (0.652 ± 0.039 vs. 0.651 ± 0.035; p = 0.629), but the seasonal decline was stronger at Odžaci (−0.0144 month^{-1}) than at Fruška Gora (−0.0050 month^{-1}). Although this trend difference was not statistically significant (interaction p = 0.117), it was directionally consistent with the poorer ICP crown condition observed at Odžaci.

Table 4. Statistical consistency between ICP crown condition and EO-derived seasonal indicators during the 2025 growing season.

EO indicator	Expected response under poorer ICP crown condition	Fruška Gora mean ± SD	Odžaci mean ± SD	p-value	FG trend month^{-1}	ODZ trend month^{-1}	Trend difference p-value	ICP–EO consistency
NDVI	Lower / stronger decline	0.859 ± 0.036	0.858 ± 0.042	0.883	−0.0053	−0.0142	0.157	Directional trend, not significant
EVI	Lower / stronger decline	0.635 ± 0.083	0.645 ± 0.070	0.467	−0.0398	−0.0462	0.483	Weak directional trend
NDRE	Lower red-edge signal / stronger decline	0.651 ± 0.035	0.652 ± 0.039	0.629	−0.0050	−0.0144	0.117	Directional trend, not significant
CIred-edge	Lower chlorophyll-related signal	3.824 ± 0.566	3.831 ± 0.667	0.586	−0.0968	−0.2556	0.103	Directional trend, not significant
MTCI	Lower chlorophyll-related signal	3.925 ± 0.581	3.775 ± 0.498	0.198	−0.1141	−0.2015	0.327	Directional level and trend, not significant
NDMI	Lower canopy moisture / stronger decline	0.329 ± 0.037	0.329 ± 0.044	0.915	−0.0217	−0.0289	**0.046**	Supported by significant trend
MSI	Higher moisture stress / stronger increase	0.507 ± 0.041	0.508 ± 0.050	0.907	+0.0245	+0.0332	**0.033**	Supported by significant trend
BSI	Higher bare-soil/canopy opening signal	−0.301 ± 0.036	−0.299 ± 0.046	0.819	+0.0208	+0.0297	**0.020**	Supported by significant trend
LAI proxy	Lower canopy density	2.179 ± 0.299	2.215 ± 0.255	0.467	−0.1438	−0.1673	0.483	Weak directional trend
FAPAR proxy	Lower canopy function	0.947 ± 0.043	0.946 ± 0.051	0.756	−0.0055	−0.0168	0.138	Directional trend, not significant
Productivity proxy	Lower productivity signal	0.816 ± 0.068	0.815 ± 0.079	0.883	−0.0101	−0.0280	0.129	Directional trend, not significant
MODIS LST Day	Higher daytime thermal stress	23.64 ± 4.69	28.49 ± 4.94	**<0.001**	+1.119	+1.130	0.981	Supported by significant mean difference

Chlorophyll-related indicators showed the same general tendency. CIred-edge had similar mean values at both plots (Odžaci: 3.831 ± 0.667; Fruška Gora: 3.824 ± 0.566; p = 0.586), but declined more

strongly at Odžaci (−0.2556 month^{-1}) than at Fruška Gora (−0.0968 month^{-1}; interaction p = 0.103). MTCI was numerically lower at Odžaci than at Fruška Gora (3.775 ± 0.498 vs. 3.925 ± 0.581; p = 0.198), and also showed a stronger seasonal decline at Odžaci (−0.2015 vs. −0.1141 month^{-1}; interaction p = 0.327). These results suggest that pigment- and red-edge-related EO indicators showed directional consistency with ICP crown condition, but without statistically significant between-plot differences.

Moisture-related indicators provided stronger support for the ICP-based interpretation. Mean NDMI values were nearly identical between Odžaci and Fruška Gora (0.329 ± 0.044 vs. 0.329 ± 0.037; p = 0.915), but the seasonal decline was significantly stronger at Odžaci (−0.0289 month^{-1}) than at Fruška Gora (−0.0217 month^{-1}; interaction p = 0.046). Similarly, mean MSI values were very similar between plots (Odžaci: 0.508 ± 0.050; Fruška Gora: 0.507 ± 0.041; p = 0.907), but MSI increased more strongly at Odžaci (+0.0332 month^{-1}) than at Fruška Gora (+0.0245 month^{-1}), and this difference in seasonal trend was statistically significant (interaction p = 0.033). This indicates that the plot with poorer ICP crown condition also showed a stronger seasonal tendency toward decreasing canopy moisture and increasing moisture stress.

The disturbance-related BSI showed a similar pattern. Mean BSI values did not differ significantly between Odžaci and Fruška Gora (−0.299 ± 0.046 vs. −0.301 ± 0.036; p = 0.819), but BSI increased more strongly at Odžaci (+0.0297 month^{-1}) than at Fruška Gora (+0.0208 month^{-1}), with a statistically significant difference in seasonal trend (interaction p = 0.020). This suggests a stronger seasonal increase in bare-soil, canopy-opening, or mixed soil–vegetation signal at Odžaci, which is consistent with the higher field-observed defoliation.

Overall, mean Sentinel-2 index values alone provided limited statistical separation between the two ICP Level II plots. In contrast, seasonal trends were more informative. The strongest ICP–EO consistency was observed for moisture- and disturbance-related indicators: NDMI declined significantly more strongly at Odžaci, while MSI and BSI increased significantly more strongly. These results indicate that the poorer ICP crown condition at Odžaci is better reflected in EO-derived seasonal trajectories than in mean optical index values alone.

To evaluate whether satellite observations followed the field-observed ICP pattern, Odžaci was treated as the plot with poorer terrestrial crown condition. EO indicators were then assessed according to whether they showed the expected response at Odžaci relative to Fruška Gora. The strongest statistical consistency was observed for moisture-, disturbance-, thermal-, and radar-related indicators. NDMI declined significantly more strongly at Odžaci, while MSI and BSI increased significantly more strongly, indicating reduced canopy moisture, increased moisture stress, and a stronger surface/canopy-opening signal at the plot with poorer crown condition. MODIS daytime LST was also significantly higher at Odžaci, and Sentinel-1 VH and VV backscatter differed significantly between the plots.

Greenness and pigment-related indicators, including NDVI, NDRE, CIred-edge, MTCI, FAPAR proxy and productivity proxy, generally changed in the expected direction but did not show statistically significant trend differences. Therefore, these indicators provide directional but weaker support. Overall, EO data did not provide a formal ICP–EO correlation because only two Level II plots were analyzed, but they showed clear exploratory consistency with the terrestrial crown-condition pattern.

Thermal indicators provided strong additional support for the interpretation of increased environmental stress at Odžaci. MODIS daytime land surface temperature during the May–September 2025 period was significantly higher at Odžaci than at Fruška Gora (Table 5). Mean daytime LST reached 28.49 ± 4.94°C at Odžaci, compared with 23.64 ± 4.69°C at Fruška Gora, and the difference was statistically significant (Mann–Whitney U test, p < 0.001). This indicates that the plot with poorer ICP crown condition was also characterized by a warmer daytime surface environment. Although LST alone cannot identify the cause of canopy decline, the elevated daytime thermal signal is consistent with reduced canopy cooling, lower water availability, or increased surface heating under stress conditions.

Structural indicators derived from Sentinel-1 radar data also showed clear between-plot differences. At Odžaci, VH backscatter averaged −16.05 ± 0.80 dB, while Fruška Gora showed higher values of −13.19 ± 3.17 dB. The difference was statistically significant ($p < 0.001$). VV backscatter showed a similar pattern, with Odžaci averaging −9.79 ± 0.75 dB and Fruška Gora −6.23 ± 3.73 dB, again with a statistically significant between-plot difference ($p < 0.001$). These radar differences indicate that the two plots differed in structural and/or moisture-related scattering properties. In the context of the field observations, the lower backscatter values at Odžaci are consistent with poorer crown condition and altered canopy structure, although radar responses should be interpreted cautiously because they are influenced by both vegetation structure and surface moisture.

Table 5. Thermal and structural EO indicators with exploratory statistical comparison.

Indicator	Odžaci	Fruška Gora	Difference ODZ–FG	Statistical test	p-value	Interpretation
MODIS LST Day mean (°C)	28.49 ± 4.94	23.64 ± 4.69	+4.85	Mann–Whitney U	<0.001	Significantly higher daytime surface temperature at Odžaci
VH backscatter (dB)	−16.05 ± 0.80	−13.19 ± 3.17	−2.86	Mann–Whitney U	<0.001	Significant structural/moisture-related radar difference
VV backscatter (dB)	−9.79 ± 0.75	−6.23 ± 3.73	−3.56	Mann–Whitney U	<0.001	Significant structural/moisture-related radar difference

4. Discussion

The combined analysis of ICP Forests field observations and satellite-derived EO indicators provided a consistent plot-scale interpretation of forest condition at the two study sites. ICP data indicated poorer crown condition at Odžaci than at Fruška Gora, with higher mean and median defoliation, fewer trees in the low-defoliation class, and more frequent recorded damage. However, recorded damage intensity did not fully explain the observed crown deterioration, confirming that defoliation should be interpreted as an integrative indicator of tree condition rather than as direct evidence of a single causal agent (Bussotti et al. 2024; Eichhorn et al. 2020).

EO indicators partly confirmed this terrestrial pattern. Mean Sentinel-2 greenness and pigment-related indices showed limited separation between the plots, which suggests that average optical index values alone were not sufficient to clearly distinguish crown condition. This is consistent with previous studies showing that vegetation indices are useful for forest monitoring but may saturate in dense canopies or respond weakly to moderate physiological stress (Huang et al. 2021; Huete, 2012; Yan et al. 2025). Therefore, forest health interpretation benefits from combining spectral, moisture, thermal and structural indicators (Drechsel and Forkel, 2025; Lausch et al. 2016; Pause et al. 2016).

Seasonal EO trajectories were more informative than seasonal mean values. Odžaci showed a significantly stronger decline in NDMI and significantly stronger increases in MSI and BSI, indicating reduced canopy moisture, increased moisture stress and a stronger surface or canopy-opening signal at the plot with poorer field-assessed crown condition. These findings are consistent with the established use of SWIR-based indices for detecting vegetation water content and forest dryness (Gao, 1996; Le et al. 2024), as well as with studies linking drought and heat stress to crown defoliation and forest decline (de la Cruz et al. 2014; Gessler et al. 2022; Michel et al. 2022).

Thermal and radar indicators provided additional support. MODIS daytime LST was significantly higher at Odžaci, suggesting a warmer daytime surface environment consistent with reduced canopy cooling, lower evapotranspiration or increased surface exposure. Sentinel-1 VH and VV backscatter were also significantly lower at Odžaci, indicating differences in structural or moisture-

related scattering properties. However, these EO signals should not be interpreted as direct proof of a specific causal driver, because LST and radar backscatter are influenced by multiple environmental and structural factors (Deshayes et al. 2006; Lausch et al. 2016; Paluba et al. 2025; Vafaei et al. 2021).

The comparison between the two plots demonstrates the added value of integrating ICP and EO data. Field observations provide tree-level information on defoliation and damage, while satellite data provide spatially and temporally explicit information on canopy greenness, moisture status, surface temperature and structural properties. Similar integrative approaches have been recommended for improving forest health monitoring and linking ground-based forest observations with EO indicators (Alekseev and Chernikhovskii, 2022; Ferretti et al. 2024; Molnár et al. 2025; Pause et al. 2016).

Overall, the strongest ICP–EO consistency was observed for moisture-related, disturbance-related, thermal and radar indicators, while greenness and pigment-related indices provided mainly directional but weaker support. Because only two ICP Level II plots were analyzed, the results should be interpreted as an exploratory consistency assessment rather than a formal correlation or regional validation. Nevertheless, the study demonstrates that EO-derived indicators can provide valuable contextual information for interpreting ICP Forests crown-condition data at plot scale, especially where field-observed defoliation is not fully explained by recorded damage intensity.

5. Conclusion

This study showed that the Odžaci ICP Level II plot had poorer terrestrial crown condition than Fruška Gora, with higher mean and median defoliation, fewer trees with low defoliation, more trees in moderate and severe defoliation classes, and more frequent recorded damage. However, the mostly low to moderate damage intensity did not fully explain the level of crown deterioration, indicating that defoliation should not be interpreted only through field-recorded damage categories.

The satellite indicators did not all respond equally to this terrestrial pattern. Mean Sentinel-2 greenness and pigment indices, including NDVI, EVI, NDRE, CIred-edge and MTCI, showed limited statistical separation between plots. In contrast, seasonal trajectories were more informative. Odžaci showed stronger declines in several vegetation and productivity-related indicators, while the clearest statistical consistency with ICP crown condition was observed for NDMI, MSI and BSI. NDMI declined more strongly at Odžaci, whereas MSI and BSI increased more strongly, indicating reduced canopy moisture, increased moisture stress and a stronger surface or canopy-opening signal.

Multi-sensor indicators strengthened this interpretation. MODIS daytime LST was significantly higher at Odžaci, and Sentinel-1 VH and VV backscatter were significantly lower, showing that the plot with poorer field-assessed crown condition also had a warmer surface environment and different structural or moisture-related radar properties. These results indicate that the EO signal associated with Odžaci was strongest in moisture, thermal, disturbance-related and radar indicators, rather than in mean greenness indices alone.

The main contribution of this study is the plot-scale integration of ICP Forests Level II observations with Sentinel-2, Sentinel-1 and MODIS indicators under Serbian monitoring conditions. The results demonstrate that EO data can support the interpretation of ICP crown-condition assessments by providing seasonal information on canopy moisture, stress development, surface temperature and structural contrast. However, because only two plots were analyzed, the findings should be considered an exploratory consistency assessment, not a formal ICP–EO correlation or regional validation. Future work should include additional ICP plots, multi-year EO time series, and independent meteorological, soil-moisture or drought-index data to confirm the environmental drivers of crown decline.

Acknowledgments

The authors gratefully acknowledge the financial support of the Ministry of Agriculture, Forestry and Water Management of the Republic of Serbia (Contract No. 000451783 2026 14844 000 000 016 012).

References

1. Ács, N., Heil, B., Szász, B., Folcz, Á., Preisinger, M., Sándor, G., Czimber, K. (2026): Two-phase forest damage assessment with Sentinel-2 NDVI double differencing and UAV-based segmentation in the Sopron Mountains. Remote Sensing 18(5): 803.
2. Alekseev, A. S., Chernikhovskii, D. M. (2022): Assessment of the state of forests based on joint statistical processing of Sentinel-2B remote sensing data and the data from network of ground-based ICP-Forests sample plots. Open Journal of Ecology 12: 513–528.
3. Bussotti, F., Potočić, N., Timmermann, V., Lehmann, M.M., Pollastrini, M. (2024): Tree crown defoliation in forest monitoring: Concepts, findings, and new perspectives for a physiological approach in the face of climate change. Forestry: An International Journal of Forest Research 97(2): 194–212.
4. de la Cruz, A.C., Gil, P.M., Fernández-Cancio, Á., Minaya, M., Navarro-Cerrillo, R.M., Sánchez-Salguero, R., Grau, J.M. (2014): Defoliation triggered by climate induced effects in Spanish ICP Forests monitoring plots. Forest Ecology and Management 331: 245–255.
5. Deshayes, M., Guyon, D., Jeanjean, H., Stach, N., Jolly, A., Hagolle, O. (2006): The contribution of remote sensing to the assessment of drought effects in forest ecosystems. Annals of Forest Science 63: 579–595.
6. Drechsel, J., Forkel, M. (2025): Remote sensing forest health assessment – a comprehensive literature review on a European level. Central European Forestry Journal 71(1): 14–39.
7. Drusch, M., Del Bello, U., Carlier, S., Colin, O., Fernandez, V., Gascon, F., Hoersch, B., Isola, C., Laberinti, P., Martimort, P., Meygret, A., Spoto, F., Sy, O., Marchese, F., Bargellini, P. (2012): Sentinel-2: ESA's optical high-resolution mission for GMES operational services. Remote Sensing of Environment 120: 25–36.
8. Eichhorn, J., Roskams, P., Potočić, N., Timmermann, V., Ferretti, M., Mues, V., Szepesi, A., Durrant, D., Seletković, I., Schröck, H.-W., Nevalainen, S., Bussotti, F., Garcia, P., Wulff, S. (2020): Part IV: Visual assessment of crown condition and damaging agents. In: UNECE ICP Forests Programme Co-ordinating Centre (ed.). Manual on methods and criteria for harmonized sampling, assessment, monitoring and analysis of the effects of air pollution on forests. Thünen Institute of Forest Ecosystems, Eberswalde, Germany, pp. 1–54.
9. Polehampton, E., Cox, C., Smith, D., Ghent, D., Wooster, M., Xu, W., Bruniquel, J., Henocq, C., Dransfeld, S. (2023): Copernicus Sentinel-3 SLSTR land user handbook. Preparation and Operations of the Mission Performance Centre (MPC) for the Copernicus Sentinel-3 Mission. European Space Agency.
10. Estrada, J. S., Fuentes, A., Reszka, P., Auat Cheein, F. (2023): Machine learning assisted remote forestry health assessment: A comprehensive state of the art review. Frontiers in Plant Science 14: 1139232.
11. Ferretti, M., Gessler, A., Cools, N., Fleck, S., Guerrieri, R., Jakovljević, T., Nicolas, M., Nieminen, T. M., Pitar, D., Potočić, N., Raspe, S., Schaub, M., Schwärzel, K., Timmermann, V., Vejpustková, M., Vesterdal, L., Vanninen, P., Waldner, P., Zimmermann, L., Sanders, T. G. M. (2024): Perspectives: Resilient forests need joint forces for better inventorying and monitoring. Forest Ecology and Management 561: 121875.
12. Galić, Z., Drekić, M., Vasić, V., Pekeč, S., Kesić, L., Novčić, Z. (2018): Monitoring temperaturnih uslova u šumskim ekosistemima na nivou II praćenja prekograničnog zagađenja u delu Republike Srbije – AP Vojvodini. Topola 201–202: 15–32.
13. Galić, Z., Karaklić, V., Samardžić, M., Novčić, Z., Drekić, M. (2025): Monitoring zemljišta na bioindikacijskim tačkama (nivo I) u AP Vojvodini, Srbija. Topola 216: 41–52.
14. Gao, B.C. (1996): NDWI – a normalized difference water index for remote sensing of vegetation liquid water from space. Remote Sensing of Environment 58(3): 257–266.

15. Gessler, A., Ferretti, M., Schaub, M. (2022): Editorial: Forest monitoring to assess forest functioning under air pollution and climate change. Frontiers in Forests and Global Change 5: 952232.
16. Ghent, D., Corlett, G., Göttsche, F.-M., Remedios, J., Trigo, I. F. (2024): The operational and climate land surface temperature products from the Sentinel-3 Sea and Land Surface Temperature Radiometer. Remote Sensing 16(18): 3403.
17. Guerrieri, R., Vanguelova, E., Munzi, S., Fotelli, M., Branquinho, C., Ferretti, M., Migliavacca, M., Salmon, Y., Ullah, S., Alonso, R., Ďurkovič, J., Fyllas, N., Machacova, K., Ostonen, I., Sarris, D., Verstraeten, A. (2025): Building synergies among ground-based forest inventorying and monitoring networks to meet scientific, political and societal needs. Plants, People, Planet.
18. Hellwig, F.M., Fluhrer, A., Dubois, C., Schellenberg, K., Chaparro, D., Zehner, M., Klosterhalfen, A., Piles, M., Schmullius, C., Kunstmann, H., Jagdhuber, T. (2026): Tracking water dynamics of a temperate forest under drought and non-drought conditions using active and passive microwave and optical remote sensing. Journal of Geophysical Research: Biogeosciences 131: e2025JG009240.
19. Hoek van Dijke, A.J., Orth, R., Teuling, A. J., Herold, M., Schlerf, M., Migliavacca, M., Machwitz, M., van Hateren, T.C., Yu, X., Mallick, K. (2023): Comparing forest and grassland drought responses inferred from eddy covariance and Earth observation. Agricultural and Forest Meteorology 341: 109635.
20. Huang, S., Tang, L., Hupy, J. P., Wang, Y., Shao, G. (2021): A commentary review on the use of normalized difference vegetation index (NDVI) in the era of popular remote sensing. Journal of Forestry Research 32: 1–6.
21. Huete, A.R. (2012): Vegetation indices, remote sensing and forest monitoring. Geography Compass 6(9): 513–532.
22. Kostić, S., Kebert, M., Todorović, H., Pekeč, S., Zorić, M., Stojanović, D.B., Orlović, S. (2022): Soil horizon-dependent heavy metals, and micro-and macro-elements distributions: A case study of Futoški park (Novi Sad, Serbia). Topola 210: 15–27.
23. Kulesza, K., Hawryło, P., Socha, J., Hościło, A. (2025): How reliable are the spectral vegetation indices for the assessment of tree condition and mortality in European temperate forests? Remote Sensing 17(15): 2549.
24. Kumar, S., Ghosh, S.S., Mandal, D., Bhattacharya, A., Porwal, A., Karthikeyan, L. (2025): Enhancing vegetation monitoring: A proposal for a Sentinel-2 based vegetation health index. Frontiers in Remote Sensing 6: 1581355.
25. Lausch, A., Erasmi, S., King, D.J., Magdon, P., Heurich, M. (2016): Understanding forest health with remote sensing – Part I. Remote Sensing 8(12): 1029.
26. Lausch, A., Erasmi, S., King, D.J., Magdon, P., Heurich, M. (2017): Understanding forest health with remote sensing – Part II. Remote Sensing 9(2): 129.
27. Le, T.S., Dell, B., Harper, R. (2024): A new remote sensing index for forest dryness monitoring using multi-spectral satellite imagery. Forests 15(6): 915.
28. Loozen, Y., Rebel, K.T., de Jong, S.M., Lu, M., Ollinger, S.V., Wassen, M. J., Karssenberg, D. (2020): Mapping canopy nitrogen in European forests using remote sensing and environmental variables with the random forests method. Remote Sensing of Environment 247: 111933.
29. Marx, A., Kleinschmit, B. (2017): Sensitivity analysis of RapidEye spectral bands and derived vegetation indices for insect defoliation detection in pure Scots pine stands. iForest – Biogeosciences and Forestry 10(4): 659–668.
30. Matović, B., Pekeč, S., Vidović, D., Drekić, M., Višacki, V., Kesić, L., Perendija, N., Vaštag, E., Orlović, S., Stojnić, S. (2024): Management practice effects on biomass and soil carbon stock in European beech (*Fagus sylvatica* L.) forests on Fruška Gora Mountain, Serbia. Topola 214: 17–34.

31. McDonald, A.J., Gemmell, F.M., Lewis, P.E. (1998): Investigation of the utility of spectral vegetation indices for determining information on coniferous forests. Remote Sensing of Environment 66(3): 250–272.
32. Michel, A., Kirchner, T., Prescher, A.-K., Schwärzel, K. (eds). (2022): Forest Condition in Europe: The 2022 Assessment. ICP Forests Technical Report. Thünen Institute.
33. Mitrović, S., Veselinović, M., Čule, N., Češljar, G., Brašanac Bosanac, Lj., Eremija, S., Petrović, U. (2021): Determination of leaf area index (LAI) at Level II sample plots according to the ICP manual. Sustainable Forestry: Collection 83–84: 65–77.
34. Molnár, T., Bolla, B., Szabó, O., Koltay, A. (2025): Sentinel-2-based forest health survey of ICP Forests Level I and II plots in Hungary. Journal of Imaging 11(11): 413.
35. Moreno-Fernández, D., Camarero, J.J., García, M., Lines, E.R., Sánchez-Dávila, J., Tijerín, J., Valeriano, C., Viana-Soto, A., Zavala, M.Á., Ruiz-Benito, P. (2022): The interplay of the tree and stand-level processes mediate drought-induced forest dieback: Evidence from complementary remote sensing and tree-ring approaches. Ecosystems 25: 1738–1753.
36. Paluba, D., Le Saux, B., Sarti, F., Štych, P. (2025): Estimating vegetation indices and biophysical parameters for Central European temperate forests with Sentinel-1 SAR data and machine learning. Big Earth Data 9(2): 155–186.
37. Pause, M., Schweitzer, C., Rosenthal, M., Keuck, V., Bumberger, J., Dietrich, P., Heurich, M., Jung, A., Lausch, A. (2016): In situ/remote sensing integration to assess forest health – a review. Remote Sensing 8(6): 471.
38. Pavlović, L., Stojanović, D. B., Kresoja, M., Stjepanović, S., Orlović, S., Bojović, M. (2017): Razvoj modela potencijalne distribucije vrsta pomoću metoda mašinskog učenja. Topola 199–200: 167–175.
39. Pelc-Mieczkowska, R. (2021): The application of Sentinel-2 data for automatic forest cover changes assessment – Białowieża Primeval Forest case study. Civil and Environmental Engineering Reports 31(4): 148–166.
40. Stojanović, D.B., Orlović, S., Zlatković, M., Kostić, S., Vasić, V., Miletić, B., Kesić, L., Matović, B., Božanić, D., Pavlović, L., Milović, M., Pekeč, S., Đurđević, V. (2021): Climate change within Serbian forests: Current state and future perspectives. Topola 208: 39–56.
41. Tanase, M.A., Mihai, M.C., Miguel, S., Cantero, A., Tijerín, J., Ruiz-Benito, P., et al. (2024): Long-term annual estimation of forest above ground biomass, canopy cover, and height from airborne and spaceborne sensors synergies. Environmental Research 259: 119432.
42. Tanovski, V., Matović, B., Kesić, L., Stojanović, D.B. (2022): A review of the influence of climate change on coniferous forests in the Balkan peninsula. Topola 210: 41–64.
43. Tigabu, A., Gessesse, A.A. (2025): Mapping forest cover change and estimating carbon stock using satellite-derived vegetation indices in Alemsaga forest, Ethiopia. PLOS ONE 20(2): e0310780.
44. Earth Resources Observation and Science (EROS) Center (2020): Landsat 8–9 Operational Land Imager/Thermal Infrared Sensor Level-2, Collection 2 [dataset]. U.S. Geological Survey.
45. Vafaei, S., Fathizadeh, O., Puletti, N., Fadaei, H., Rasooli, S.B., Vaglio Laurin, G. (2021): Estimation of forest leaf area index using satellite multispectral and synthetic aperture radar data in Iran. iForest – Biogeosciences and Forestry 14(3): 278–284.
46. Vasić, V., Drekić, M., Poljaković Pajnik, L., Vasić, S., Kesić, L., Galić, Z. (2020): Sastav prizemne flore na bioindikacijskoj tački nivoa II na Fruškoj gori. Topola 206: 35–40.
47. Vulova, S., Horn, K., Rocha, A.D., Brill, F., Somogyvári, M., Okujeni, A., Förster, M., Kleinschmit, B. (2025): Unraveling the response of forests to drought with explainable artificial intelligence (XAI). Ecological Indicators 172: 113308.
48. Yan, K., Gao, S., Yan, G., Ma, X., Chen, X., Zhu, P., Li, J., Gao, S., Gastellu-Etchegorry, J.-P., Myneni, R.B., Wang, Q. (2025): A global systematic review of the remote sensing vegetation indices. International Journal of Applied Earth Observation and Geoinformation 136: 104560.